PASJ: Publ. Astron. Soc. Japan **60**, L27–L30, 2008 October 25

Spectroscopic Confirmation of the Fifth Image of SDSS J1004+4112 and Implications for the $M_{\rm BH}$–σ_* Relation at $z = 0.68$*

Naohisa INADA,[1] Masamune OGURI,[2] Emilio E. FALCO, [3] Tom J. BROADHURST,[4] Eran O. OFEK,[5]
Christopher S. KOCHANEK,[6] Keren SHARON,[4] and Graham P. SMITH[7]
[1]*Cosmic Radiation Laboratory, RIKEN, 2-1 Hirosawa, Wako, Saitama 351-0198*
[2]*Kavli Institute for Particle Astrophysics and Cosmology, Stanford University, Menlo Park, CA 94025, USA*
[3]*Harvard-Smithsonian Center for Astrophysics, 60 Garden Street, Cambridge, MA 02138, USA*
[4]*School of Physics and Astronomy, Tel Aviv University, Tel Aviv 69978, Israel*
[5]*Department of Astronomy, 105-24, California Institute of Technology, Pasadena, California 91125, USA*
[6]*Department of Astronomy, The Ohio State University, Columbus, OH 43210, USA*
[7]*School of Physics and Astronomy, University of Birmingham, Edgbaston, Birmingham, B152TT, UK*

(Received 2008 July 24; accepted 2008 August 7)

Abstract

We present the results of deep spectroscopy for the central region of the cluster lens SDSS J1004+4112 with the Subaru Telescope. A secure detection of an emission line of the faint blue stellar object (component E) near the center of the brightest cluster galaxy (G1) confirms that it is the central fifth image of the lensed quasar system. In addition, we measured the stellar velocity dispersion of G1 to be $\sigma_* = 352 \pm 13\,{\rm km\,s^{-1}}$. We combined these results to obtain constraints on the mass $M_{\rm BH}$ of the putative black hole (BH) at the center of the inactive galaxy G1, and hence on the $M_{\rm BH}$–σ_* relation at the lens redshift $z_{\rm l} = 0.68$. From detailed mass modeling, we placed an upper limit on the black hole mass, $M_{\rm BH} < 2.1 \times 10^{10} M_\odot$ at the 1σ level ($< 3.1 \times 10^{10} M_\odot$ at 3σ), which is consistent with black hole masses expected from the local and redshift-evolved $M_{\rm BH}$–σ_* relations, $M_{\rm BH} \sim 10^9$–$10^{10} M_\odot$.

Key words: black hole physics — galaxies: elliptical and lenticular, cD — galaxies: quasars: individual (SDSS J1004+4112) — gravitational lensing

1. Introduction

Quasars lensed by foreground clusters of galaxies serve as a powerful probe of the mass distributions of clusters. SDSS J1004+4112 is the first example of such quasar-cluster lens systems (Inada et al. 2003; Oguri et al. 2004; Ota et al. 2006). It consists of four bright quasar images ($z = 1.734$) with a maximum image separation of $14\farcs6$, produced by a massive cluster at $z = 0.68$. In addition to the quasar images, multiply imaged background galaxies were also observed (Sharon et al. 2005). An advantage for using lensed quasars is that they can provide time delays, which have actually been detected for this system (Fohlmeister et al. 2007, 2008), containing unique information on the lens potential.

What makes the quasar lens SDSS J1004+4112 particularly unique is a probable central fifth image (component E) of the lensed quasar system. High-resolution Hubble Space Telescope (HST) Advanced Camera for Survey (ACS; Clampin 2000) images show a blue point source located $0\farcs2$ from the center of the brightest cluster galaxy G1 (Inada et al. 2005). The central lensed image, if confirmed, has several important implications for the central structure of lensing objects. For instance, central images can constrain the inner mass profiles of lensing galaxies, particularly the masses of the central supermassive black holes (e.g., Mao et al. 2001; Rusin & Ma 2001; Keeton 2003; Rusin et al. 2005). While a correlation between the black hole mass ($M_{\rm BH}$) and the stellar velocity dispersions (σ_*) of the host galaxies has been established for local galaxies (Ferrarese & Merritt 2000; Gebhardt et al. 2000; Tremaine et al. 2002), measurements of the redshift evolution for the correlation, derived for galaxies hosting active galactic nuclei, are still controversial (e.g., Peng et al. 2006; Shen et al. 2008; Woo et al. 2008). Thus, independent constraints from central images are thought to provide insights into this relation.

In this Letter, we present results of two deep spectroscopic follow-up observations for SDSS J1004+4112, conducted at the Subaru 8.2 m telescope. One is the spectroscopy of component E to confirm its lensing nature, and the other is the spectroscopy of galaxy G1 to measure its velocity dispersion. The latter observation is particularly important in separating the mass distribution of dark matter from that of baryons (e.g., Sand et al. 2008). We thus attempted mass modeling of the lens system. Together with a measurement of σ_* for galaxy G1, it provides a direct constraint on the $M_{\rm BH}$–σ_* relation at a lens redshift of $z = 0.68$. In what follows, we assume a standard flat universe with $\Omega_M = 0.26$, $\Omega_\Lambda = 0.74$, and $H_0 = 72\,{\rm km\,s^{-1}\,Mpc^{-1}}$ (e.g., Tegmark 2006).

* Based on data collected at Subaru Telescope, which is operated by the National Astronomical Observatory of Japan, and observations (GO-9774, GO-10509, and GO-10716) made with the NASA/ESA Hubble Space Telescope, obtained at the Space Telescope Science Institute, which is operated by the Association of Universities for Research in Astronomy, Inc., under NASA contract NAS 5-26555.

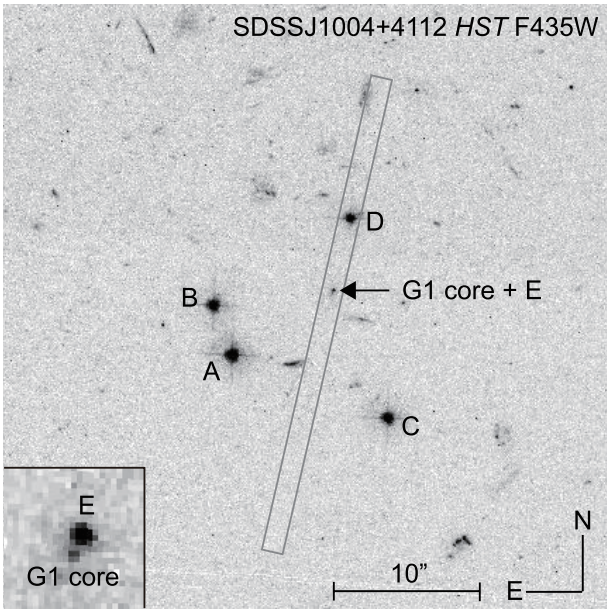

Fig. 1. HST ACS F435W image of SDSS J1004+4112 with an exposure time of 5400 s, taken on 2005 December 19 under the GO-10509 program (PI: C. S. Kochanek). Components labeled by A–D indicate the 4 lensed quasar images, and "G1 core + E" indicates the central fifth image E and the center of galaxy G1. The gray rectangle shows the slit direction for spectroscopy of the fifth image. The inset shows an expanded view of the central region of galaxy G1. North is up and East is left, and the pixel scale is $0\farcs05$ pixel^{-1}. See Inada et al. (2005) for HST images in other (redder) bands.

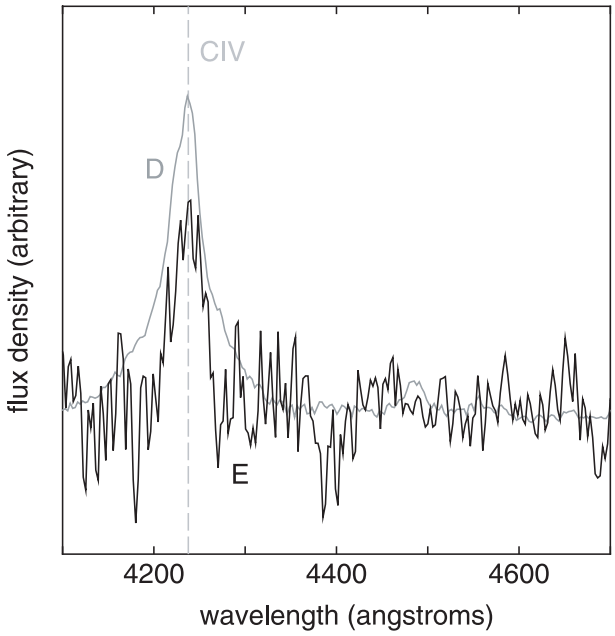

Fig. 2. Spectra of components E (black) and D (gray), normalized by each continuum level. In component E, an emission line is detected at the same wavelength as the C IV emission line of component D (also indicated by a vertical dotted line). The origin of the absorption features around 4200 Å and 4400 Å are unknown.

2. Observations and Data Analysis

2.1. *Fifth Image*

We conducted spectroscopic observations of the central fifth image (component E; see figure 1) with the Faint Object Camera And Spectrograph (FOCAS: Kashikawa et al. 2002) at the Subaru 8.2-meter telescope on 2007 January 22. We used the 300B grism, the L600 filter, and a $1\farcs0$-width slit, under the 2×2 (spatial $\times$ spectral) on-chip binning mode. With this configuration the wavelength coverage was from 3650 Å to 6000 Å, which covered a strong emission line (C IV) of the lensed quasar with a spectral resolution of R $\sim$ 400 and a pixel scale of $0\farcs207$ pixel^{-1}. Although component E is quite close to the center of galaxy G1 at $z = 0.68$ ($0\farcs2$ from the center of G1), our blue spectroscopy minimized any contamination from G1. The slit direction was aligned so as to pass through component D ($\sim 10\farcs0$ from component E, see figure 1) of SDSS J1004+4112, which we adopted as a reference for the quasar emission lines. Given the faintness ($B \sim 24.5$) of component E, we used a total exposure time of 16200 s, taken under excellent seeing conditions (FWHM of $\sim 0\farcs6$). After removing cosmic rays using the Lacos_spec task (van Dokkum 2001), we extracted 1-dimensional spectra of components E and D using the standard IRAF tasks. The spectra, normalized by the continuum level of each image, are shown in figure 2. We find that the spectrum of component E shows a clear emission line just at the wavelength of the C IV emission line of component D. We note that there is no sky emission line near the wavelength of the C IV emission line (4200 Å). Thus, our spectroscopic observations unambiguously confirm that component E is the central fifth image of the lens system, representing the first spectroscopic confirmation of central odd images among lensed quasars.

2.2. *Velocity Dispersion of G1*

To measure the velocity dispersion of galaxy G1, we also used FOCAS, but with a different setup. We adopted the 600–650 VPH grism (High 650), the SY47 filter, and a $0\farcs4$-width slit. The wavelength coverage in this setup was from 5300 Å to 7700 Å, covering the Ca II H&K and G-band absorption lines of galaxy G1 at $z = 0.68$. The slit direction was aligned along the major axis of galaxy G1 (160°.8 East of North). The spectrum, with a total exposure of 21600 s, was obtained on 2007 January 21, under the 3×1 on-chip binning mode (a spatial scale of $0\farcs311$ pixel^{-1}). The setup was chosen to achieve a spectral resolution of R $\sim$ 2500. The seeing was $\sim 0\farcs7$ FWHM. Again, cosmic rays were removed by the Lacos_spec task and the 1-dimensional spectrum of galaxy G1 was extracted by the standard IRAF tasks.

We measured the velocity dispersion of G1 following the procedure described in Falco et al. (1997). We adopted HD 8491, HD 83085, HD 94247, and HD 126778 in the coudé feed spectral library (Valdes et al. 2004) as template stars. We rebinned and smoothed the template spectra to match the observed spectral resolutions of our data. Both the spectrum of G1 and the resolution-matched template stars were normalized by the continuum levels. We then applied the Fourier cross-correlation method (Tonry & Davis 1979) of the IRAF FXCOR task to templates convolved with Gaussians. The resultant calibration curves describe the relation between the input velocity dispersion and the FWHM of the output cross-correlation peak

measured by the FXCOR task. We used velocity dispersions from 200 km s^{-1} to 450 km s^{-1} with an interval of 10 km s^{-1}. The FXCOR task was also applied to the normalized rest-frame spectrum of G1 to obtain the width of the G-band absorption line,[1] which we converted to the velocity dispersion using a linear interpolation of the calibration curves. We found that 4 template stars yield similar velocity dispersions for G1 of 338–367 km s^{-1}. From the average and scatter (no weight for the 4 independent measurements), we determined the velocity dispersion to be $\sigma_* = 352 \pm 13$ km s^{-1}. Our measurement is consistent with σ_* expected from the observed Faber–Jackson relation, $\sim 320 \pm 40$ km s^{-1} (Liu et al. 2008).

3. Constraints on the $M_{\rm BH}$–σ_* Relation

The location and the brightness of the confirmed central image allow us to place constraints on the mass of the supermassive BH hosted by G1. This is made possible by the fact that central point masses (de-)magnify, or even suppress, central images (e.g., Mao et al. 2001; Rusin et al. 2005). Indeed, the technique was applied to a three-image galaxy-scale lens, PMN J1632−0033, to derive an upper limit on $M_{\rm BH}$ in the lensing galaxy (Winn et al. 2004), although a lack of any redshift measurement for the lensing galaxy made an interpretation of this result somewhat difficult.

Before conducting detailed mass modeling, we could estimate the BH mass range from the distance between component E and the center of G1. It is given by the mass at which the Einstein radius of the central BH becomes comparable to this distance of $\sim 0\farcs2$, corresponding to a BH mass of $M_{\rm BH} \sim 1.5 \times 10^{10} M_\odot$. Thus, we naively expected $M_{\rm BH} \lesssim 10^{10} M_\odot$.

To obtain more quantitative constraints, we fit the quasar images with the following mass model. We adopt an elliptical version of the (NFW: Navarro et al. 1997) density profile for the dark-matter distribution of the lensing cluster. Changing the inner slope of the dark-matter component is expected to have little effect on the fifth image, because the center of the dark halo appears to be offset from G1 (Oguri et al. 2004). The central position, ellipticity, position angle, concentration parameter, and total mass of the dark-matter distribution were treated as free parameters. The central galaxy G1 was assumed to be an isothermal ellipsoid with varying core radius. We constrained the position angle so as to coincide with that of the light ($161^\circ \pm 10^\circ$ East of North), but with no prior constraint on the ellipticity. In addition we added a Gaussian prior on the velocity dispersion of the isothermal ellipsoid G1 from our measurement, $\sigma = 352 \pm 13$ km s^{-1}. The 16 galaxies other than G1, which we identified as cluster members using their colors, are included as truncated isothermal ellipsoids with an exact scaling relation, $\sigma_* \propto L^{1/4}$ and $r_{\rm trunc} \propto L^{1/2}$. The overall normalization of $r_{\rm trunc}$ is left as a free parameter. We took the ellipticities and position angles for these member galaxies from measurements in the HST ACS images. Finally, we allowed for an external shear following Oguri et al. (2004) to achieve better fits. For observational constraints, we adopted the positions and position errors of five quasar images and G1 derived in Inada et al. (2005). We also included the flux ratios of quasar images as constraints, but with large errors of $\sigma(m_{\rm X} - m_{\rm A}) = 0.3$ (X represents images B–D) and $\sigma(m_{\rm E} - m_{\rm A}) = 0.8$, in order to allow for small flux ratio changes due to time delays and

[1] The G-band is the only line which we can use, because the Ca II H and K absorption lines are not suitable for measuring velocity dispersions (Tonry 1998; Ohyama et al. 2002).

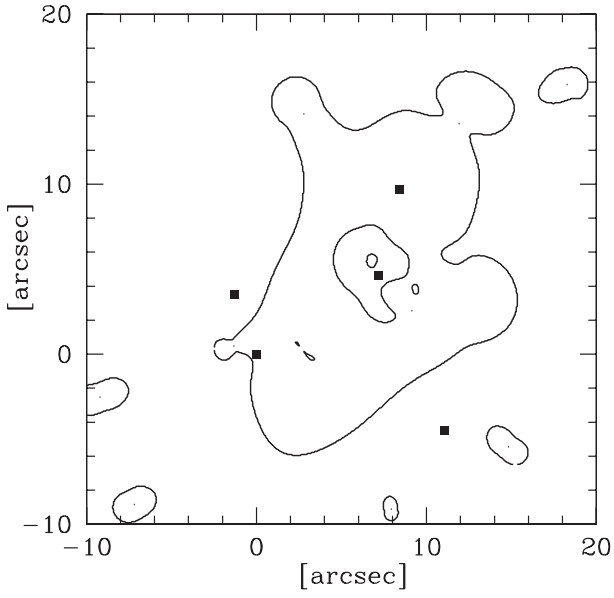

Fig. 3. Critical curves of our best-fit mass model. The observed positions of five quasar images are marked by filled squares, which were reproduced by our model nearly perfectly. The best-fit parameters are $M_{\rm NFW} = 2 \times 10^{15} M_\odot$, $c_{\rm NFW} = 2$, $x_{\rm NFW} = 6\farcs184$, $y_{\rm NFW} = 6\farcs639$, $e_{\rm NFW} = 0.3$, $\theta_{\rm NFW} = -11^\circ$, $e_{\rm G1} = 0.71$, $\theta_{\rm G1} = 152^\circ$, $\sigma_{\rm G1} = 355$ km s^{-1}, $r_{\rm core,G1} = 0\farcs1$, $\gamma = 0.21$, $\theta_\gamma = 82^\circ$, and $r_{\rm trunc}(L = L_{\rm G1}) = 3\farcs2$.

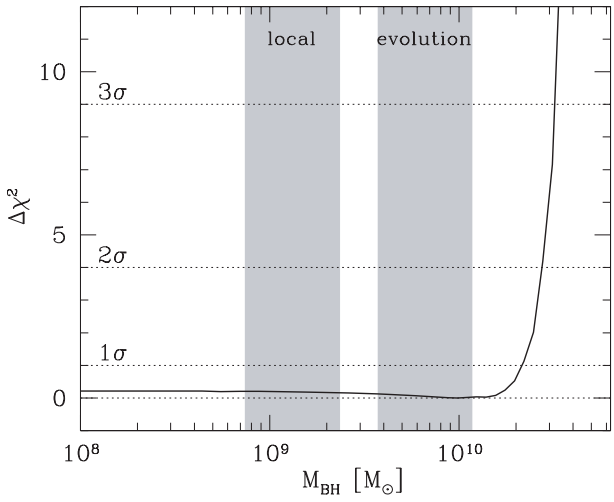

Fig. 4. The χ^2 difference ($\Delta\chi^2$) as a function of the BH mass $M_{\rm BH}$. The steep rise of $\Delta\chi^2$ provides upper limits on $M_{\rm BH}$. The shaded regions indicate the values of $M_{\rm BH}$ expected from the measured stellar velocity dispersion $\sigma_* = 352 \pm 13$ km s^{-1}: The "local" value is estimated from the $M_{\rm BH}$–σ_* relation of Tremaine et al. (2002), $M_{\rm BH} = 10^{8.13} (\sigma_*/200\,{\rm km\,s^{-1}})^{4.02} M_\odot$ with an intrinsic dispersion of ~ 0.25 dex, whereas the "evolution" value is computed in the same way as "local", except for an additional offset of the BH mass due to a possible redshift evolution measured by Woo et al. (2008), $\Delta \log M_{\rm BH} = 3.1 \log(1+z) = 0.70$ for $z = 0.68$.

microlensing. In addition, the observed time delays, $\Delta t_{\rm AB} = 40.6 \pm 1.8$ d (Fohlmeister et al. 2007) and $\Delta t_{\rm AC} = 821.6 \pm 2.1$ d (Fohlmeister et al. 2008), were included.

We found that our model reproduces the data quite well (see figure 3 for the critical curves of our best-fit model). With no BH, the best-fit chi-square is $\chi^2 = 2.57$ for 3° of freedom (20 constraints and 17 parameters). Thus, the central BH is not required to fit the fifth image. We then placed the BH (modeled by a point mass) at the center of galaxy G1, and re-performed χ^2 minimizations for each $M_{\rm BH}$. We note that the central BH can produce a sixth image near the BH. In what follows we ignore the sixth image, since it is much fainter than the observed fifth image in most of the situations considered here. We derived the upper limit of $M_{\rm BH}$ from the χ^2 differences, $\Delta\chi^2 = \chi^2(M_{\rm BH}) - \chi^2_{\rm min}$. Figure 4 plots $\Delta\chi^2$ as a function of $M_{\rm BH}$, from which we derived constraints on the BH mass of $M_{\rm BH} < 2.1 \times 10^{10} M_\odot$ at 1σ and $M_{\rm BH} < 3.1 \times 10^{10} M_\odot$ at 3σ. The steep increase of χ^2 for large $M_{\rm BH}$ means that the mass of the BH is limited to being a small fraction of the stellar mass interior to image E.

As shown in figure 4, our constraints on $M_{\rm BH}$ are consistent with the expected local $M_{\rm BH}$–σ_* relation (Tremaine et al. 2002), and also those inferred from the extrapolation of a possible redshift evolution measured by Woo et al. (2008). Although the constraints are model-dependent, in the sense that they are derived assuming a specific parametric mass model, we note that our mass model is quite flexible near the center of G1 because the core radius is a free parameter. Indeed, the best-fit core radius is correlated with $M_{\rm BH}$; the core radius evolves from $\sim 0\farcs1$ for $M_{\rm BH} = 0$ to $\sim 0\farcs3$ for $M_{\rm BH} = 3 \times 10^{10} M_\odot$. The rough agreement of this constraint with a simple order-of-magnitude argument also suggests that the upper limit to the BH mass of approximately $2 \times 10^{10} M_\odot$ is generic. However, improved constraints may be obtained by adding constraints on the sixth image, which we ignored, because it becomes brighter with increasing $M_{\rm BH}$. For instance, the flux of the sixth image is $\sim$20% of E in our best-fit models for $M_{\rm BH} \sim 2 \times 10^{10} M_\odot$, whereas the HST image suggests that it cannot be $\gtrsim 10\%$ of E.

4. Summary

We have presented the results of two spectroscopic observations at the Subaru telescope. With the first observation, we confirmed that the central point source found by Inada et al. (2005) is indeed the central fifth image of the lensed quasar by detecting the C IV emission line of the quasar. This represents the first spectroscopic confirmation of the central odd image. In the second spectroscopic observation, we determined the stellar velocity dispersion of galaxy G1 to be $\sigma_* = 352 \pm 13\,{\rm km\,s^{-1}}$.

We used these results to derive constraints on the $M_{\rm BH}$–σ_* relation at a lens redshift of $z = 0.68$, assuming the presence of a BH at the center of the brightest cluster galaxy, G1. With a parametric model that successfully reproduces the model constraints, we obtained limits of $M_{\rm BH} < 2.1 \times 10^{10} M_\odot$ at 1σ and $M_{\rm BH} < 3.1 \times 10^{10} M_\odot$ at 3σ that are consistent with $M_{\rm BH}$ expected from extrapolation of the known $M_{\rm BH}$–σ_* relation. It is worth noting that these constraints were derived for an "inactive" galaxy with no nuclear activity. Current studies of the redshift evolution of the $M_{\rm BH}$–σ_* relation make use of the Balmer line widths, and therefore are restricted to BHs in active galaxies. Given possible differences in the $M_{\rm BH}$–σ_* between active and inactive local galaxies (Greene & Ho 2006), constraints on $M_{\rm BH}$ for distant inactive galaxies from gravitational lensing will be essential to fully understand the origin of the relation.

N. I. acknowledges support from the Special Postdoctoral Researcher Program of RIKEN. This work was in part supported by Department of Energy contract DE-AC02-76SF00515. C. S. K. acknowledges support from NSF grant AST 07-08082. G. P. S acknowledges support from a Royal Society University Research Fellowship. E. F. acknowledges support from the Smithsonian Institution.

References

Clampin, M., et al. 2000, Proc. SPIE, 4013, 344
Falco, E. E., Shapiro, I. I., Moustakas, L. A., & Davis, M. 1997, ApJ, 484, 70
Ferrarese, L., & Merritt, D. 2000, ApJ, 539, L9
Fohlmeister, J., et al. 2007, ApJ, 662, 62
Fohlmeister, J., Kochanek, C. S., Falco, E. E., Morgan, C. W., & Wambsganss, J. 2008, ApJ, 676, 761
Gebhardt, K., et al. 2000, ApJ, 539, L13
Greene, J. E., & Ho, L. C. 2006, ApJ, 641, L21
Inada, N., et al. 2003, Nature, 426, 810
Inada, N., et al. 2005, PASJ, 57, L7
Kashikawa, N., et al. 2002, PASJ, 54, 819
Keeton, C. R. 2003, ApJ, 582, 17
Liu, F. S., Xia, X. Y., Mao, S., Wu, H., & Deng, Z. G. 2008, MNRAS, 385, 23
Mao, S., Witt, H. J., & Koopmans, L. V. E. 2001, MNRAS, 323, 301
Navarro, J. F., Frenk, C. S., & White, S. D. M. 1997, ApJ, 490, 493
Oguri, M., et al. 2004, ApJ, 605, 78
Ohyama, Y., et al. 2002, AJ, 123, 2903
Ota, N., et al. 2006, ApJ, 647, 215
Peng, C. Y., Impey, C. D., Rix, H.-W., Kochanek, C. S., Keeton, C. R., Falco, E. E., Lehár, J., & Mcleod, B. A. 2006, ApJ, 649, 616
Rusin, D., Keeton, C. R., & Winn, J. N. 2005, ApJ, 627, L93
Rusin, D., & Ma, C.-P. 2001, ApJ, 549, L33
Sand, D. J., Treu, T., Ellis, R. S., Smith, G. P., & Kneib, J.-P. 2008, ApJ, 674, 711
Sharon, K., et al. 2005, ApJ, 629, L73
Shen, J., Vanden Berk, D. E., Schneider, D. P., & Hall, P. B. 2008, AJ, 135, 928
Tegmark, M., et al. 2006, Phys. Rev. D, 74, 123507
Tonry, J. L. 1998, AJ, 115, 1
Tonry, J., & Davis, M. 1979, AJ, 84, 1511
Tremaine, S., et al. 2002, ApJ, 574, 740
Valdes, F., Gupta, R., Rose, J. A., Singh, H. P., & Bell, D. J. 2004, ApJS, 152, 251
van Dokkum, P. G. 2001, PASP, 113, 1420
Winn, J. N., Rusin, D., & Kochanek, C. S. 2004, Nature, 427, 613
Woo, J.-H., Treu, T., Malkan, M. A., & Blandford, R. D. 2008, ApJ, 681, 925